VERSITA

Central European Journal of Chemistry
DOI: 10.2478/s11532-006-0033-1
**Research article**
CEJC 4(4) 2006 646–665

# Hybrid density functional theory investigation of a series of alloxan-based thiosemicarbazones and semicarbazones

N.W.S.V. Nuwan De Silva, Edward C. Lisic, Titus V. Albu*

*Department of Chemistry,*
*Tennessee Technological University,*
*Cookeville, Tennessee 38505*

Received 15 May 2006; accepted 19 June 2006

**Abstract:** Recently, the synthesis and the NMR characterization of a series of eight alloxan-based thiosemicarbazones and semicarbazones were reported. These compounds exhibit a strongly hydrogen-bonded hydrazinic proton that is a part of a characteristic six-membered ring. This proton is highly deshielded and resonates far downfield in the proton NMR spectra. In this report, mPW1PW91/6-31+G(d,p) calculations have been used to investigate the structure and other molecular properties of this series of eight compounds. The relationship between the $^{1}$H and $^{13}$C NMR chemical shifts and various geometric parameters was investigated, and linear relationships for proton peaks that are involved in hydrogen-bond interactions were found.


*Keywords: Alloxan, thiosemicarbazones, NMR chemical shifts, hybrid density functional theory*

## 1 Introduction

Thiosemicarbazones (TSC) and their complexes with transition metals have gained considerable interest due to their antitumor effects, antiviral activities, and their anticancer activity [1–5]. For example, phenanthrenequinone thiosemicarbazone acts as a tridentate ligand and reacts easily with $Pd^{2+}$ to form a square planar metal complex that has potent antitumor properties [6] and $Cu^{2+}$ and $Zn^{2+}$ acenaphthenequinone TSC metal complexes have antiviral activity [7]. In addition, electronic accessibility was related to the oxidant property of these compounds, thus emphasizing the importance of the TSC moiety in antithyroid therapy [8].

* E-mail: albu@tntech.edu

In synthesizing new TSC molecules, there is a special interest in utilizing bioactive starting materials with interesting backbone moieties that have vicinal carbonyls. Alloxan or 2,4,5,6(1*H*,3*H*)-pyrimidinetetrone is especially interesting because it has been reported as a potent agent for the selective destruction of pancreatic $\beta$-cells of mice, which can induce permanent diabetes. Evidence indicates that the pancreatic $\beta$-cell damage induced by alloxan occurs through the generation of cytotoxic oxygen free radicals, and the primary target of free radical species seems to be the DNA of pancreatic $\beta$-cells [9–11]. However, the alloxan-induced $\beta$-cell damage due to the fragmentation of DNA by alloxan is inhibited in the presence of glucose [12]. Similarly, one can imagine that alloxan-thiosemicarbazone compounds will have the ability to interact with DNA. Alloxan-thiosemicarbazone was found to be active in vitro against a wide variety of bacteria, yeasts, and molds that are pathogenic to animals and plants, and was also used in formulating mold-resistant vinyl coatings and plasticizers [13].

Our work focuses on the synthesis and characterization of new TSC ligands and their subsequent reactions with specific metal ions [14–16]. Recently, we reported the synthesis and NMR characterization of a series of eight alloxan-based thiosemicarbazones and semicarbazones [16]. (Two of the compounds in this series have been synthesized previously.[13]) The synthesis of these compounds was carried out in dry isopropanol by reacting alloxan with the appropriate thiosemicarbazide or semicarbazide in presence of catalytic amounts of concentrated sulfuric acid. These compounds show a characteristic far-downfield resonance in the proton NMR spectrum as a result of intramolecular hydrogen bonding. The same moiety was observed in other classes of TSC compounds, such as the 1,2-naphthoquinone 5-sulfonic acid TSC, phenanthrenequinone TSC, acenaphthenequinone TSC, and isatin sulfonic acid TSC [14, 15].

Theoretical studies can further advance the understanding of the molecular properties of TSC compounds and their complexes with transitional metals, and few such studies have been reported recently [17–21]. Some studies have focused on optimized geometries and conformational distribution [18, 20] while others have focused on NMR properties [17, 19, 21].

In this study, the results of a hybrid density functional theory investigation into the structures and molecular properties of a series of eight thiosemicarbazones and semicarbazones are presented. The purpose of this study is two-fold since not only are the NMR chemical shifts of these compounds calculated but correlations with various molecular properties are also examined. The results will be used to unequivocally assign some $^{1}$H and $^{13}$C chemical shifts that are experimentally more difficult to interpret.

## 2 Computational methodologies

The level of electronic structure theory used in this study is mPW1PW91 [22] in conjunction with the 6-31+G(d,p) basis set. The mPW1PW91 method is a hybrid density functional theory method that employs a 25% Hartree-Fock exchange contribution, the modified Perdew-Wang (mPW) exchange functional [22] and the PW91 correlation func-

tional [23]. This hybrid density functional theory method gives accurate molecular properties like geometries, vibrational frequencies, and enthalpies of formation. It has been also shown to give accurate NMR chemical shifts [24, 25].

All investigated systems are closed-shell systems, and the calculations were carried out using restricted wave functions. The molecular optimizations were carried out using tight convergence criteria to properly define the molecular geometries. The optimized geometries were determined to be true energy minima (not saddle points) by vibrational analysis that yielded no imaginary frequencies. The NMR chemical shifts were obtained from Gauge-Independent Atomic Orbital (GIAO) calculations [26–28] at the same level of theory, mPW1PW91/6-31+G(d,p), as the geometry optimization. To converts the chemical shifts to ppm and compare them with the experimental values, we subtracted the calculated isotropic values from the calculated isotropic values of $^{1}$H and $^{13}$C in optimized TMS (31.6515 and 196.597, respectively) at the same level of theory. We also calculated atomic charges based on Mulliken population analysis [29–32] and generalized atomic polar tensor (GAPT) methodology [33–35]. All electronic structure calculations were carried out using the Gaussian 03 suite of programs [36].

## 3 Results

Our study focused on a series of eight alloxan-based compounds comprising six thiosemicarbazones and two semicarbazones: alloxan thiosemicarbazone (**1**) denoted ALL-TSC, alloxan methylthiosemicarbazone (**2**) denoted ALL-MTSC, alloxan ethylthiosemicarbazone (**3**) denoted ALL-ETSC, alloxan benzylthiosemicarbazone (**4**) denoted ALL-BzTSC, alloxan phenylthiosemicarbazone (**5**) denoted ALL-PTSC, alloxan dimethylthiosemicarbazone (**6**) denoted ALL-DMTSC, alloxan semicarbazone (**7**) denoted ALL-SC, and alloxan phenylsemicarbazone (**8**) denoted ALL-PSC [37]. The optimized structures of these compounds are shown in Figure 1 while the numbering scheme of the alloxan (thio)semicarbazone moiety and the definition of $H_A$ - $H_E$ protons are given in Figure 2.

The results of this study are presented in 4 tables and 10 figures. Table 1 gives selected optimized geometrical parameters for the studied compounds, and Table 2 lists calculated GAPT and Mulliken atomic charges of selected atoms. All other Mulliken atomic charges are available in the Supplementary Information [38]. Table 3 lists selected experimental and calculated $^{1}$H NMR chemical shifts, and Table 4 lists calculated $^{13}$C NMR chemical shifts for all investigated compounds. Figures 3 and 8 present calculated $^{1}$H NMR chemical shifts versus experimental $^{1}$H NMR chemical shifts for $H_A$ and $H_D$, respectively. Figures 4-6 and 9-11 show calculated and/or experimental $^{1}$H NMR chemical shifts as a function of particular geometric parameters. Figures 7 and 12 present calculated $^{1}$H NMR chemical shifts versus calculated GAPT atomic charges for $H_A$ and $H_D$, respectively. In Figure 1 and all figures showing results, we used a color-labeling scheme as follows: ALL-TSC (**1**) results are given in blue, ALL-MTSC (**2**) results are given in light blue, ALL-ETSC (**3**) results are given in pale blue, ALL-BzTSC (**4**) results are given in lime, ALL-PTSC (**5**) results are given in dark yellow, ALL-DMTSC (**6**) re-

sults are given in green, ALL-SC (**7**) results are given in red, and ALL-PSC (**8**) results are given in orange.

## 4 Discussion

The mPW1PW91/6-31+G(d,p) calculations show that six of the investigated compounds (ALL-TSC, ALL-MTSC, ALL-ETSC, ALL-PTSC, ALL-SC, and ALL-PSC) have a planar structure (i.e., $C_s$ symmetry) while two compounds (ALL-BzTSC and ALL-DMTSC) are non-planar. This observation is also clear when inspecting the optimized molecular geometries shown in Figure 1. In one of these non-planar molecules, ALL-DMTSC, the C5′–N4′–C3′–N2′ and the C6′–N4′–C3′–N2′ dihedral angles are 20.88 and –169.85 degrees, respectively. These dihedral angles are a measure of how much the carbon atoms (of the two methyl groups) are out of plane with the other atoms. In the optimized structure of the other non-planar molecule, ALL-BzTSC, the C7′–C6′–C5′–N4′ dihedral angle, which is a measure of the angle the plane of the benzene ring is making with the plane of the alloxan ring, is 97.7 degrees. Selected geometric parameters for all the optimized structures are given in Table 1 and full Cartesian coordinates are available as Supplementary Information [38].

In addition to determining optimized molecular geometries for ALL-TSC and ALL-SC, we investigated the process of rotation around the C3′–N4′ single bond (that interchanges $H_D$ and $H_E$) and determined the transition state along this torsional coordinate. The conventional transition state (i.e., the saddle point) has $C_s$ symmetry for both compounds, with $H_D$ and $H_E$ being equivalent. N4′ is $sp^2$ hybridized (i.e., planar) in the optimized structures and $sp^3$ hybridized in the transition state. For ALL-TSC, the classical (i.e., the zero-point exclusive) barrier height is 21.02 kcal/mol, the zero-point inclusive barrier height is 20.16 kcal/mol, and the imaginary frequency at the saddle point is 477.6 $i$ cm$^{-1}$. The C3′–N4′–$H_D$ and C3′–N4′–$H_E$ angles are both equal to 110.16 degrees, the $H_D$–N4′–$H_E$ angle is 105.52 degrees, and the N2′–C3′–N4′–$H_D$ and N2′–C3′–N4′–$H_E$ dihedrals are ±58.00 degrees. Similarly, for ALL-SC, the classical (i.e., the zero-point exclusive) barrier height is 18.46 kcal/mol, the zero-point inclusive barrier height is 17.84 kcal/mol, and the imaginary frequency at the saddle point is 452.6 $i$ cm$^{-1}$. The C3′–N4′–$H_D$ and C3′–N4′–$H_E$ angles are both equal to 110.08 degrees, $H_D$–N4′–$H_E$ angle is 105.38 degrees, and N2′–C3′–N4′–$H_D$ and N2′–C3′–N4′–$H_E$ dihedrals are ±57.87 degrees. The high calculated barrier heights of rotation suggest that the two protons ($H_D$ and $H_E$) are not easily interchangeable on the NMR time scale, and therefore they should give distinct NMR signals. Experimentally it was observed that indeed the ALL-TSC NMR spectrum presents two distinct $^1$H signals at 9.503 and 8.614 ppm while ALL-SC presents only one signal, equivalent to two protons, at 7.355 ppm.

In the case of ALL-DMTSC, the two methyl groups bonded to N4′ are also determined to be nonequivalent in the optimized structure. Their interchange involves rotation around the C3′–N4′ single bond. We identified the transition state for this interchange, and we determined that it has $C_s$ symmetry with both methyl groups equivalent. For

this transition state, the C5′–N4′–C3′–N2′ and the C6′–N4′–C3′–N2′ dihedral angles are ±115.36 degrees. The classical (i.e., the zero-point exclusive) barrier height is 15.36 kcal/mol, the zero-point inclusive barrier height is 14.65 kcal/mol, and the imaginary frequency at the saddle point is 112.7 $i$ cm$^{-1}$. The high calculated barrier height implies a rather slow interchange and therefore distinct $^{13}$C NMR signals for each methyl group.

Besides determining structural parameters for the investigated compounds, the main goal of this study is to gain a better understanding of the molecular properties determining the NMR behavior of these thiosemicarbazones and semicarbazones. Our focus was on four $^{1}$H and five $^{13}$C NMR signals.

The hydrazinic proton $H_A$ was investigated in more detail because it appears at large chemical shifts (12.8 to 14.2 ppm), mainly due to strong hydrogen-bonding interaction with the carbonyl oxygen atom. This behavior has been observed in other thiosemicarbazones that we have synthesized [14, 15] as well as others [39]. The atoms of interest for investigating the geometry around this proton are coplanar for all investigated compounds except ALL-BzTSC and ALL-DMTSC that show slightly twisted structures with the O(4)–C4···N2′–$H_A$ dihedral angle of 0.04 degrees in ALL-BzTSC and 5.59 degrees in ALL-DMTSC, respectively. The small dihedral angles show that even those structures can be considered, for purpose of discussion, as coplanar.

A plot of the calculated vs. the experimental NMR chemical shifts for $H_A$ protons for all the compounds investigated show a good linear relationship (Figure 3) implying that the methodology employed here is appropriate for studying these compounds. The two semicarbazones (**7** and **8**) show a slightly different behavior than the thiosemicarbazones but similar enough to allow us to investigate all eight compounds as just one series. Both the calculated and the experimental NMR chemical shifts of $H_A$ protons with respect to various geometric parameters of the optimized geometries were explored in more depth, and we found especially good linear relationships with the N2′–$H_A$ distance (Figure 4) and the O(4)···$H_A$ distance (Figure 5) although the data is somewhat scattered in the latter case. The chemical shift of $H_A$ appear further downfield as the N2′–$H_A$ distance increases and the O(4)···$H_A$ distance decreases. These tendencies can be understood in terms of the hydrogen-bond interaction that exists between O(4) and $H_A$. A stronger hydrogen-bond interaction will shorten the O(4)···$H_A$ distance and will elongate the N2′–$H_A$ distance and will also causes a significant deshielding of the $H_A$ proton leading to further downfield NMR signal.

There are also good correlations between the calculated NMR chemical shifts of $H_A$ in thiosemicarbazones and the N2′···O(4) distance or the N2′–$\ddot{H}_A$O(4) angle (Figure 6). In these correlations, the semicarbazones (**7** and **8**) have a slightly different behavior and appear more as outliers. However, they follow the same general trends of calculated $H_A$ chemical shift decreasing with the N2′···O(4) distance and increasing with the N2′–$\ddot{H}_A$O(4) angle. We also found (although no plots are shown) that the experimental chemical shift of $H_A$ in thiosemicarbazones is proportional with the N1′–N2′–C3′ angle and inversely proportional with the $H_A$–N2′–C3′ angle and the S···$H_A$ distance. (Again, the semicarbazones show similar behavior but appear as outliers of the thiosemicarbazone results.)

The inversely proportional behavior of experimental $H_A$ chemical shift vs. $S\cdots H_A$ distance implies that hydrogen-bond interaction between S and $H_A$ may also be significant. Based on these results, one can conclude that the local geometry near the $H_A$ proton is a determining factor in its NMR properties. A good linear correlation between calculated or experimental chemical shifts of $H_A$ and the calculated Mulliken charges of $H_A$ was not found. This is most likely due to the limitations of Mulliken charge calculations that are known to be basis set dependent and employ an equal partition of the charge between the bonded atoms. However, plotting the calculated chemical shift versus the more physical GAPT atomic charges gives a linear representation showing the expected inverse proportionality behavior (Figure 7).

It is also interesting to compare the results for ALL-TSC with those for ALL-SC as well as the results of ALL-PTSC with those for ALL-PSC because comparing these compounds allows one to determine the effects of replacing S with O. Based simply on electronegativity arguments, one would expect that the more electronegative O would attract electron density better than S therefore deshielding $H_A$ to a greater extend. This would make the chemical shift appear further downfield for ALL-SC compared to ALL-TSC, and ALL-PSC compared to ALL-PTSC. For both pairs, the chemical shift of $H_A$ is actually further downfield for thiosemicarbazones. The difference $[\delta_{H_A}(\text{ALL - TSC}) - \delta_{H_A}(\text{ALL - SC})]$ is 0.546 for both experimentally determined and calculated shifts, while $[\delta_{H_A}(\text{ALL - PTSC}) - \delta_{H_A}(\text{ALL - PSC})]$ is 0.367 for experimentally determined shifts and 0.319 for calculated shifts. These are excellent correlations between experimental and calculated values and are consistent with the calculated Mulliken charges (but not with the GAPT charges) of $H_A$ that are slightly more positive for thiosemicarbazones than semicarbazones.

The other important proton for the compounds investigated here is $H_D$. This proton is present in only seven out of eight compounds (ALL-DMTSC does not have this proton). A plot of the calculated vs. the experimental NMR chemical shifts for $H_D$ protons is shown in Figure 8. Although the correlation is not perfectly linear, the figure clearly shows a proportional relationship between the calculated and experimental chemical shift values. The $H_D$ proton is also involved in a hydrogen-bond interaction with N1′. One would therefore expect behavior similar to the $H_A$ proton. Indeed, from Figures 9 and 10, one can see that the chemical shift for $H_D$ increases as the N4′–$H_D$ distance increases and as the N1′$\cdots H_D$ distance decreases. The data however appears more scattered than in the case of $H_A$ proton. Also the $H_D$ chemical shift increases as the N1′$\cdots$N4′ distance decreases and as N1′$\cdots H_D$–N4′ increases (Figure 11). Similar to $H_A$, we did not find a good linear correlation between calculated and experimental chemical shifts of $H_D$ and the calculated Mulliken or GAPT charges of $H_D$. For illustration purposes, we show the representation of calculated $H_D$ chemical shifts vs. the GAPT charges in Figure 12.

The two protons bonded to nitrogen in the alloxan ring ($H_B$ and $H_C$) are equivalent in alloxan but are distinct in all thiosemicarbazones and semicarbazones investigated here. Calculations allow a proper assignment of the experimentally observed NMR signals. The alloxan ring protons resonate around 11.9 ppm and 11.6 ppm. Although the calculated

chemical shifts of $H_B$and $H_C$ are not in a very good agreement with the experimental values, the GIAO calculations show consistently that $H_B$ chemical shift will appear further downfield that $H_C$ chemical shift. Based on these results, one can properly assign the chemical shifts around 11.9 to $H_B$ and the chemical shift around 11.6 to $H_C$.

Theoretical calculations also include the $^{13}$C NMR chemical shifts that are given in Table 4. The results can be used to accurately assign the NMR signals especially for the carbon atoms in alloxan ring. The results show that the downfield signals at 155.5 ppm and 152.5 ppm arise from C4 and C6. The chemical shift of C4 is calculated to be consistently higher that that of C6 by about 3 ppm. The signal for C2 is calculated to appear at about 142.1 ppm. The most upfield signal is obtained for C5 between 110.8 and 114.3 ppm. Also important is the chemical shift for C3′ that is calculated to be further downfield for thiosemicarbazones (at 167.6-178.6 ppm) than for semicarbazones (at 144.3 and 146.3 ppm).

## 5 Summary and concluding remarks

This paper presents the results of a computational study at the mPW1PW91/6-31+G(d,p) level of theory of a series of eight thiosemicarbazones and semicarbazones. We investigated various molecular properties including the optimized structures, selected rotational barrier heights, and $^1$H and $^{13}$C NMR chemical shifts.

Hydrogen-bond interactions are responsible for remarkable downfield $^1$H NMR peaks for this series of compounds. The most important hydrogen-bond interaction for $H_A$ is with O(4) but interaction with S(3′) in thiosemicarbazones or O(3′) in semicarbazones could also be significant. For $H_D$, the hydrogen-bond interaction is with N1′. The strength of hydrogen-bond interaction is manifested in different local geometries (mainly internuclear distances but also bond angles) about $H_A$ and $H_D$ and in the downfield NMR chemical shifts for these protons. Various linear relationships between the chemical shifts and selected geometric parameters have been observed. $^{13}$C NMR chemical shifts were also calculated and reported, and these results can be used for assigning experimentally observed $^{13}$C NMR signals.

## Acknowledgment

The authors appreciate the support in carrying out this research provided by the College of Arts and Sciences at Tennessee Technological University.

## References

[1] S. Padhye and G.B. Kauffman: “Transition metal complexes of semicarbazones and thiosemicarbazones”, *Coord. Chem. Rev.*, Vol. 63, (1985), pp. 127–160.

[2] D.X. West, S.B. Padhye and P.B. Sonawane: “Structural and physical correlations

in the biological properties of transition metal heterocyclic thiosemicarbazone and S-alkyl dithiocarbazate complexes", *Struct. Bonding*, Vol. 76, (1991), pp. 1–50.

[3] D.X. West, A.E. Liberta, S.B. Padhye, R.C. Chikate, P.B. Sonawane, A.S. Kumbhar and R.G. Yerande: "Thiosemicarbazone complexes of copper(II): structural and biological studies", *Coord. Chem. Rev.*, Vol. 123, (1993), pp. 49–71.

[4] T. Varadinova, D. Kovala-Demertzi, M. Rupelieva, M. Demertzis and P. Genova: "Antiviral activity of platinum (II) and palladium (II) complexes of pyridine-2-carbaldehyde thiosemicarbazone", *Acta Virol.*, Vol. 45, (2001), pp. 87–94.

[5] D. Kovala-Demertzi, M.A. Demertzis, J.R. Miller, C. Papadopoulou, C. Dodorou and G. Filousis: "Platinum(II) complexes with 2-acetylpyridine thiosemicarbazone. Synthesis, crystal structure, spectral properties, antimicrobial and antitumour activity", *J. Inorg. Biochem.*, Vol. 86, (2001), pp. 555–563.

[6] S. Padhye, Z. Afrasiabi, E. Sinn, J. Fok, K. Mehta and N. Rath: "Antitumor metallothiosemicarbazonates: Structure and antitumor activity of palladium complex of phenanthrenequinone thiosemicarbazone", *Inorg. Chem.*, Vol. 44, (2005), pp. 1154–1156.

[7] M.C. Rodriguez-Arguelles, M.B. Ferrari, G.G. Fava, C. Pelizzi, G. Pelosi, R. Albertini, A. Bonati, P.P. Dall'Aglio, P. Lunghi and S. Pinelli: "Acenaphthenequinone thiosemicarbazone and its transition metal complexes: synthesis, structure, and biological activity", *J. Inorg. Biochem.*, Vol. 66, (1997), pp. 7–17.

[8] R.R.A. Abou-Shaaban: "Atom-level electrotopological state indexes of thiourylene-type compounds and their antioxidant/oxidant properties: A novel immunoregulatory-guideline", *Saudi Pharm. J.*, Vol. 4, (1996), pp. 10–22.

[9] H. Yamamoto, Y. Uchigata and H. Okamoto: "DNA strand breaks in pancreatic islets by in vivo administration of alloxan or streptozotocin", *Biochem. Biophys. Res. Commun.*, Vol. 103, (1981), pp. 1014–1020.

[10] H. Okamoto: "Molecular basis of experimental diabetes: degeneration, oncogenesis and regeneration of pancreatic B-cells of islets of Langerhans", *Bio Essays*, Vol. 2, (1985), pp. 15–21.

[11] N. Takasu, T. Asawa, I. Komiya, Y. Nagasawa and T. Yamada: "Alloxan-induced DNA strand breaks in pancreatic islets. Evidence for hydrogen peroxide as an intermediate", *J. Biol. Chem.*, Vol. 266, (1991), pp. 2112–2114.

[12] H.-W. Rho, J.-N. Lee, H.-R. Kim, B.-H. Park and J.-W. Park: "Protective mechanism of glucose against alloxan-induced b-cell damage: pivotal role of ATP", *Exp. Mol. Med.*, Vol. 32, (2000), pp. 12–17.

[13] J.D. Douros, Jr., M. Brokl and A.F. Kerst: Gates Rubber Co., US 3773952, 1973.

[14] J.W. Carter, R. Mayes, K.A. Pierce, R. Lawson and E.C. Lisic: "Structural determination of a series of ortho-quinone thiosemicarbazone compounds using NMR spectroscopy", *J. Und. Chem. Res.*, Vol. 2, (2003), pp. 73–77.

[15] T. Bell, R. Mayes, R. Lawson and E.C. Lisic: "Synthesis of a series of isatin-3-thiosemicarbazone-5-sulfonic acid compounds and structural characterization using NMR spectroscopy", *J. Und. Chem. Res.*, Vol. 3, (2004), pp. 39–45.

[16] E.C. Lisic, R.R. Nareddy, R. Huxford and E.C. Lisic: "Synthesis of a series of isatin-3-thiosemicarbazone-5-sulfonic acid compounds and structural characterization using NMR spectroscopy", *J. Und. Chem. Res.*, Vol. 5, (2006), pp. 61–66.

[17] C. Paiola, R. Cammi, P. Pelagatti and C. Pelizzi: "A density functional theory study of structural and NMR properties of SNN thiosemicarbazone ligands and their Pd(II) chlorocomplexes", *Theochem*, Vol. 623, (2003), pp. 105–119.

[18] A.M.B. Bastos, A.F.d.C. Alcantara and H. Beraldo: "Structural analyses of 4-benzoylpyridine thiosemicarbazone using NMR techniques and theoretical calculations", *Tetrahedron*, Vol. 61, (2005), pp. 7045–7053.

[19] H. Yüksek, I. Cakmak, S. Sadi, M. Alkan and H. Baykara: "Synthesis and GIAO NMR calculations for some novel 4-heteroarylidenamino-4,5-dihydro-1*H*-1,2,4-triazol-5-one derivatives: Comparison of theoretical and experimental $^{1}$H- and $^{13}$C-chemical shifts", *Int. J. Mol. Sci.*, Vol. 6, (2005), pp. 219–229.

[20] F.F. Jian, P.S. Zhao, Z.S. Bai and L. Zhang: "Quantum chemical calculation studies on 4-phenyl-1-(propan-2-ylidene)thiosemicarbazide", *Struct. Chem.*, Vol. 16, (2005), pp. 635–639.

[21] H. Yüksek, O. Gürsoy, I. Cakmak and M. Alkan: "Synthesis and GIAO NMR calculations for some new 4,5-dihydro-1*H*-1,2,4-triazol-5-one derivatives: Comparison of theoretical and experimental $^{1}$H and $^{13}$C chemical shifts", *Magn. Reson. Chem.*, Vol. 43, (2005), pp. 585–587.

[22] C. Adamo and V. Barone: "Exchange functionals with improved long-range behavior and adiabatic connection methods without adjustable parameters: the mPW and mPW1PW models", *J. Chem. Phys.*, Vol. 108, (1998), pp. 664–675.

[23] J.P. Perdew, J.A. Chevary, S.H. Vosko, K.A. Jackson, M.R. Pederson, D.J. Singh and C. Fiolhais: "Atoms, molecules, solids, and surfaces: applications of the generalized gradient approximation for exchange and correlation", *Phys. Rev. B*, Vol. 46, (1992), pp. 6671–6687.

[24] K.B. Wiberg: "Comparison of density functional theory models' ability to reproduce experimental $^{13}$C-NMR shielding values", *J. Comp. Chem.*, Vol. 20, (1999), pp. 1299–1303.

[25] T.H. Sefzik, D. Turco, R.J. Iuliucci and J.C. Facelli: "Modeling NMR chemical shift: A survey of density functional theory approaches for calculating tensor properties", *J. Phys. Chem. A*, Vol. 109, (2005), pp. 1180–1187.

[26] H.F. Hameka: "Theory of magnetic properties of molecules, with particular emphasis on the hydrogen molecule", *Rev. Mod. Phys.*, Vol. 34, (1962), pp. 87–101.

[27] R. Ditchfield: "Self-consistent perturbation theory of diamagnetism. I. A gage-invariant LCAO(linear combination of atomic orbitals) method for NMR chemical shifts", *Mol. Phys.*, Vol. 27, (1974), pp. 789–807.

[28] K. Wolinski, J.F. Hinton and P. Pulay: "Efficient implementation of the gauge-independent atomic orbital method for NMR chemical shift calculations", *J. Am. Chem. Soc.*, Vol. 112, (1990), pp. 8251–8260.

[29] R.S. Mulliken: "Electronic population analysis on LCAO-MO molecular wave func-

tions. I", *J. Chem. Phys.*, Vol. 23, (1955), pp. 1833–1840.

[30] R.S. Mulliken: "Electronic population analysis on LCAO-MO molecular wave functions. II. Overlap populations, bond orders, and covalent bond energies", *J. Chem. Phys.*, Vol. 23, (1955), pp. 1841–1846.

[31] R.S. Mulliken: "Electronic population analysis on LCAO-MO molecular-wave functions. III. Effects of hybridization on overlap and gross AO populations", *J. Chem. Phys.*, Vol. 23, (1955), pp. 2338–2342.

[32] R.S. Mulliken: "Electronic population analysis on LCAO-MO molecular-wave functions. IV. Bonding and antibonding in LCAO and valence-bond theories", *J. Chem. Phys.*, Vol. 23, (1955), pp. 2343–2346.

[33] J. Cioslowski: "A new population analysis based on atomic polar tensors", *J. Am. Chem. Soc.*, Vol. 111, (1989), pp. 8333–8336.

[34] J. Cioslowski, T. Hamilton, G. Scuseria, B.A. Hess, Jr., J. Hu, L.J. Schaad and M. Dupuis: "Application of the GAPT (generalized atomic polar tensor) population analysis to some organic molecules and transition structures", *J. Am. Chem. Soc.*, Vol. 112, (1990), pp. 4183–4186.

[35] J. Cioslowski, P.J. Hay and J.P. Ritchie: "Charge distributions and effective atomic charges in transition-metal complexes using generalized atomic polar tensors and topological analysis", *J. Phys. Chem.*, Vol. 94, (1990), pp. 148–151.

[36] Gaussian 03, Revision B.02, M.J. Frisch, G.W. Trucks, H.B. Schlegel, G.E. Scuseria, M.A. Robb, J.R. Cheeseman, J. Montgomery, J. A.; , T. Vreven, K.N. Kudin, J.C. Burant, J.M. Millam, S.S. Iyengar, J. Tomasi, V. Barone, B. Mennucci, M. Cossi, G. Scalmani, N. Rega, G.A. Petersson, H. Nakatsuji, M. Hada, M. Ehara, K. Toyota, R. Fukuda, J. Hasegawa, M. Ishida, T. Nakajima, Y. Honda, O. Kitao, H. Nakai, M. Klene, X. Li, J.E. Knox, H.P. Hratchian, J.B. Cross, C. Adamo, J. Jaramillo, R. Gomperts, R.E. Stratmann, O. Yazyev, A.J. Austin, R. Cammi, C. Pomelli, J.W. Ochterski, P.Y. Ayala, K. Morokuma, G.A. Voth, P. Salvador, J.J. Dannenberg, V.G. Zakrzewski, S. Dapprich, A.D. Daniels, M.C. Strain, O. Farkas, D.K. Malick, A.D. Rabuck, K. Raghavachari, J.B. Foresman, J.V. Ortiz, Q. Cui, A.G. Baboul, S. Clifford, J. Cioslowski, B.B. Stefanov, G. Liu, A. Liashenko, P. Piskorz, I. Komaromi, R.L. Martin, D.J. Fox, T. Keith, M.A. Al-Laham, C.Y. Peng, A. Nanayakkara, M. Challacombe, P.M.W. Gill, B. Johnson, W. Chen, M.W. Wong, C. Gonzalez and J.A. Pople, Gaussian, Inc., Pittsburgh PA, 2003.

[37] IUPAC names: ALL-TSC = pyrimidine-2,4,5,6(1*H*,3*H*)-tetrone 5-thiosemicarbazone, ALL-MTSC = pyrimidine-2,4,5,6(1*H*,3*H*)-tetrone 5-(*N*-methylthiosemicarbazone), ALL-ETSC = pyrimidine-2,4,5,6(1*H*,3*H*)-tetrone 5-(*N*-ethylthiosemicarbazone), ALL-BzTSC = pyrimidine-2,4,5,6(1*H*,3*H*)-tetrone 5-(*N*-benzylthiosemicarbazone), ALL-PTSC = pyrimidine-2,4,5,6(1*H*,3*H*)-tetrone 5-(*N*-phenylthiosemicarbazone), ALL-DMTSC = pyrimidine-2,4,5,6(1*H*,3*H*)-tetrone 5-(*N*,*N*-dimethylthiosemicarbazone), ALL-SC = pyrimidine-2,4,5,6(1*H*,3*H*)-tetrone 5-semicarbazone, and ALL-PSC = pyrimidine-2,4,5,6(1*H*,3*H*)-tetrone 5-(*N*-phenylsemicarbazone).

[38] The Supplementary Information includes geometries in Cartesian coordinates, calculated isotropic magnetic shielding tensors, energies, and frequencies for all stationary points optimized in this work and the Mulliken atomic charges for the minimum structures. This material is available upon request from the corresponding author. E-mail your inquiries to albu@tntech.edu.

[39] D.X. West, A.K. El-Sawaf and G.A. Bain: "Metal complexes of N(4)-substituted analogs of the antiviral drug methisazone {1-methylisatin thiosemicarbazone}", *Transit. Metal Chem.*, Vol. 23, (1998), pp. 1–6.

**Table 1** Selected geometric parameters calculated at the mPW1PW91/6-31+G(d,p) level of theory.

| | ALL-TSC | ALL-MTSC | ALL-ETSC | ALL-BzTSC | ALL-PTSC | ALL-DMTSC | ALL-SC | ALL-PSC |
|---|---|---|---|---|---|---|---|---|
| Distances (A) | | | | | | | | |
| N1–$H_B$ | 1.011 | 1.011 | 1.011 | 1.011 | 1.011 | 1.011 | 1.011 | 1.011 |
| N3–$H_C$ | 1.012 | 1.012 | 1.012 | 1.012 | 1.012 | 1.012 | 1.012 | 1.012 |
| C5–N1′ | 1.304 | 1.305 | 1.306 | 1.306 | 1.305 | 1.307 | 1.303 | 1.304 |
| N1′–N2′ | 1.299 | 1.296 | 1.295 | 1.296 | 1.294 | 1.298 | 1.296 | 1.295 |
| N2′–C3′ | 1.399 | 1.406 | 1.407 | 1.406 | 1.414 | 1.409 | 1.421 | 1.426 |
| C3′–N4′ | 1.335 | 1.332 | 1.331 | 1.331 | 1.340 | 1.340 | 1.345 | 1.350 |
| C3′–S/O(3′) | 1.652 | 1.655 | 1.656 | 1.656 | 1.653 | 1.663 | 1.214 | 1.215 |
| N2′–$H_A$ | 1.024 | 1.024 | 1.024 | 1.025 | 1.025 | 1.026 | 1.024 | 1.024 |
| O(4)···$H_A$ | 1.908 | 1.908 | 1.913 | 1.901 | 1.915 | 1.886 | 1.913 | 1.909 |
| N2′···O(4) | 2.652 | 2.651 | 2.654 | 2.648 | 2.655 | 2.650 | 2.653 | 2.651 |
| S/O(3′)···$H_A$ | 2.755 | 2.749 | 2.746 | 2.745 | 2.698 | 2.687 | 2.496 | 2.480 |
| N4′–$H_D$ | 1.011 | 1.013 | 1.014 | 1.014 | 1.018 | – | 1.008 | 1.013 |
| N1′···$H_D$ | 2.205 | 2.155 | 2.157 | 2.182 | 2.037 | – | 2.260 | 2.141 |
| N4′···N1′ | 2.591 | 2.602 | 2.604 | 2.611 | 2.576 | 2.772 | 2.630 | 2.625 |
| Angles (degree) | | | | | | | | |
| N2′–$H_A$···O(4) | 126.8 | 126.8 | 126.6 | 127.1 | 126.4 | 128.6 | 126.6 | 126.7 |
| N4′–$H_D$···N1′ | 100.7 | 104.6 | 104.5 | 03.4 | 110.5 | – | 100.0 | 107.2 |
| C5–C4–O(4) | 123.4 | 123.4 | 123.5 | 123.5 | 123.4 | 123.6 | 123.5 | 123.4 |
| N1′–C5–C4 | 123.8 | 123.7 | 123.7 | 123.7 | 123.6 | 124.1 | 123.7 | 123.6 |
| N2′–N1′–C5 | 122.2 | 122.3 | 122.4 | 122.1 | 122.7 | 121.4 | 122.4 | 122.5 |
| N1′–N2′–$H_A$ | 121.2 | 121.2 | 121.3 | 121.1 | 121.2 | 119.9 | 121.3 | 121.1 |
| N1′–N2′–C3′ | 119.6 | 119.9 | 119.9 | 120.0 | 120.5 | 121.6 | 120.2 | 120.8 |
| N2′–C3′–N4′ | 114.3 | 114.4 | 114.4 | 114.6 | 112.1 | 117.6 | 114.4 | 113.3 |
| N4′–C3′–S/O(3′) | 126.8 | 127.2 | 127.3 | 127.0 | 131.5 | 126.4 | 127.1 | 129.0 |
| N2′–C3′–S/O(3′) | 118.9 | 118.5 | 118.3 | 118.3 | 116.4 | 116.0 | 118.5 | 117.8 |
| C3′–N4′–$H_D$ | 120.5 | 116.9 | 117.0 | 117.8 | 112.9 | – | 121.1 | 115.1 |
| N1′···N4′–$H_D$ | 56.7 | 53.2 | 53.3 | 54.4 | 47.8 | – | 57.8 | 51.2 |
| N2′–N1′···$H_D$ | 84.9 | 84.2 | 84.2 | 84.1 | 84.1 | – | 84.3 | 83.6 |
| C3′–N2′···$H_A$ | 119.3 | 119.0 | 118.9 | 118.9 | 118.4 | 117.0 | 118.5 | 118.0 |

**Table 2** Calculated generalized atomic polar tensor (GAPT) and selected Mulliken atomic charges for the investigated compounds.

| | ALL-TSC | ALL-MTSC | ALL-ETSC | ALL-BzTSC | ALL-PTSC | ALL-DMTSC | ALL-SC | ALL-PSC |
|---|---|---|---|---|---|---|---|---|
| GAPT | | | | | | | | |
| C6 | 1.359 | 1.357 | 1.351 | 1.328 | 1.333 | 1.341 | 1.286 | 1.285 |
| N1 | -0.922 | -0.924 | -0.925 | -0.929 | -0.942 | -0.920 | -0.901 | -0.928 |
| C2 | 1.594 | 1.595 | 1.595 | 1.595 | 1.615 | 1.589 | 1.559 | 1.593 |
| N3 | -0.945 | -0.949 | -0.950 | -0.950 | -0.970 | -0.947 | -0.915 | -0.948 |
| C4 | 1.146 | 1.165 | 1.174 | 1.196 | 1.237 | 1.173 | 1.167 | 1.244 |
| C5 | -0.781 | -0.812 | -0.821 | -0.828 | -0.886 | -0.818 | -0.672 | -0.784 |
| O(6) | -0.804 | -0.801 | -0.796 | -0.776 | -0.773 | -0.795 | -0.790 | -0.768 |
| $H_B$ | 0.248 | 0.247 | 0.246 | 0.243 | 0.245 | 0.244 | 0.245 | 0.244 |
| O(2) | -0.968 | -0.975 | -0.978 | -0.982 | -0.996 | -0.979 | -0.937 | -0.970 |
| $H_C$ | 0.241 | 0.241 | 0.241 | 0.242 | 0.245 | 0.239 | 0.242 | 0.246 |
| O(4) | -0.700 | -0.707 | -0.709 | -0.717 | -0.724 | -0.713 | -0.746 | -0.762 |
| N1′ | 0.676 | 0.673 | 0.669 | 0.653 | 0.678 | 0.699 | 0.566 | 0.596 |
| N2′ | -0.861 | -0.860 | -0.859 | -0.862 | -0.877 | -0.838 | -0.886 | -0.932 |
| $H_A$ | 0.251 | 0.249 | 0.248 | 0.250 | 0.254 | 0.243 | 0.256 | 0.259 |
| C3′ | 1.315 | 1.267 | 1.295 | 1.398 | 1.409 | 1.294 | 1.692 | 1.772 |
| S/O(3′) | -0.617 | -0.593 | -0.602 | -0.630 | -0.587 | -0.650 | -0.926 | -0.875 |
| N4′ | -0.788 | -0.785 | -0.829 | -0.920 | -0.895 | -0.752 | -0.809 | -0.975 |
| $H_D$ (R)[a] | 0.292 | 0.252 | 0.250 | 0.258 | 0.268 | (0.287) | 0.292 | 0.270 |
| $H_E$ (R)[a] | 0.264 | (0.361) | (0.400) | (0.431) | (0.366) | (0.300) | 0.278 | (0.435) |
| | | | | | | | | |
| Mulliken | | | | | | | | |
| $H_A$ | 0.395 | 0.393 | 0.394 | 0.395 | 0.401 | 0.393 | 0.392 | 0.399 |
| $H_D$ (R)[a] | 0.373 | 0.383 | 0.381 | 0.391 | 0.366 | (0.157) | 0.365 | 0.357 |

[a] R represents the substituent group. The charge given in the table (in parenthesis) is the sum of all the atoms in that group.

**Table 3** Experimental and calculated $^1$H NMR chemical shifts (ppm) [a].

| Compound | $H_A$ | | $H_B$ | | $H_C$ | | $H_D(H_E)$ | |
|---|---|---|---|---|---|---|---|---|
| | exp | calc | exp | calc | exp | calc | exp | calc |
| Thiosemicarbazones | | | | | | | | |
| ALL-TSC (1) | 13.406 | 13.280 | 11.779 | 7.134 | 11.558 | 7.060 | 9.503<br>(8.614) | 7.712<br>(6.215) |
| ALL-MTSC (2) | 13.532 | 13.347 | 11.783 | 7.144 | 11.575 | 6.981 | 9.467 | 7.932 |
| ALL-ETSC (3) | 13.523 | 13.288 | 11.766 | 7.106 | 11.550 | 7.024 | 9.424 | 7.735 |
| ALL-BzTSC (4) | 13.621 | 13.394 | 11.778 | 7.046 | 11.558 | 6.941 | 9.926 | 7.634 |
| ALL-PTSC (5) | 13.791 | 13.255 | 11.856 | 7.158 | 11.630 | 7.032 | 11.180 | 10.171 |
| ALL-DMTSC (6) | 14.251 | 13.522 | 11.787 | 7.071 | 11.522 | 6.923 | – | – |
| Semicarbazones | | | | | | | | |
| ALL-SC (7) | 12.860 | 12.734 | 11.636 | 7.134 | 11.440 | 6.985 | 7.355<br>(7.355) | 6.534<br>(4.461) |
| ALL-PSC (8) | 13.424 | 12.936 | 11.673 | 7.144 | 11.467 | 7.030 | 10.413 | 8.489 |

[a] The experimental results are obtained in DMSO-$d^6$, the calculated results are in gas phase.

**Table 4** Calculated $^{13}$C NMR chemical shifts (ppm).

| Compound | C2 | C4 | C5 | C6 | C3′ |
|---|---|---|---|---|---|
| Thiosemicarbazones | | | | | |
| ALL-TSC (1) | 142.027 | 155.142 | 111.997 | 152.467 | 175.991 |
| ALL-MTSC (2) | 142.173 | 155.334 | 111.464 | 152.375 | 174.904 |
| ALL-ETSC (3) | 142.280 | 155.006 | 111.318 | 152.762 | 173.515 |
| ALL-BzTSC (4) | 142.118 | 155.611 | 111.850 | 152.019 | 173.000 |
| ALL-PTSC (5) | 142.148 | 155.864 | 110.842 | 153.245 | 167.637 |
| ALL-DMTSC (6) | 142.222 | 155.440 | 112.488 | 153.146 | 178.580 |
| Semicarbazones | | | | | |
| ALL-SC (7) | 142.124 | 155.652 | 114.321 | 152.182 | 146.348 |
| ALL-PSC (8) | 142.263 | 156.463 | 113.776 | 152.829 | 144.291 |

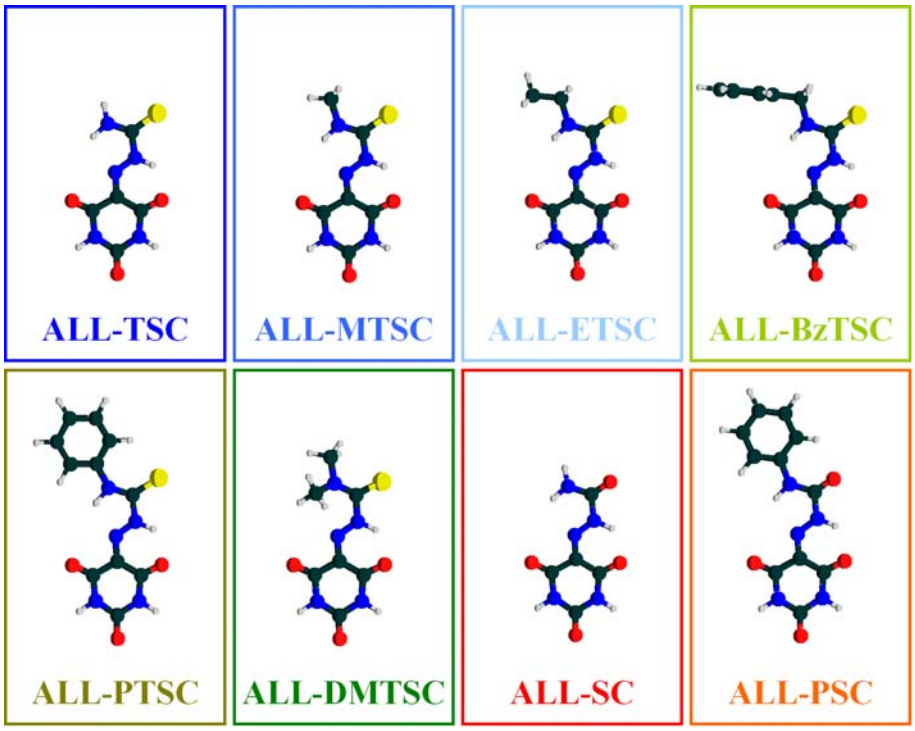


**Fig. 1** Optimized structures of studied thiosemicarbazones and semicarbazones.

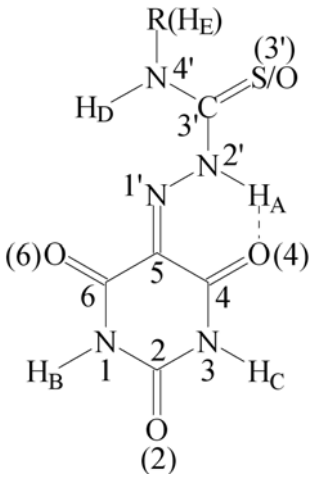


**Fig. 2** The numbering scheme and the proton labeling in the investigated compounds.

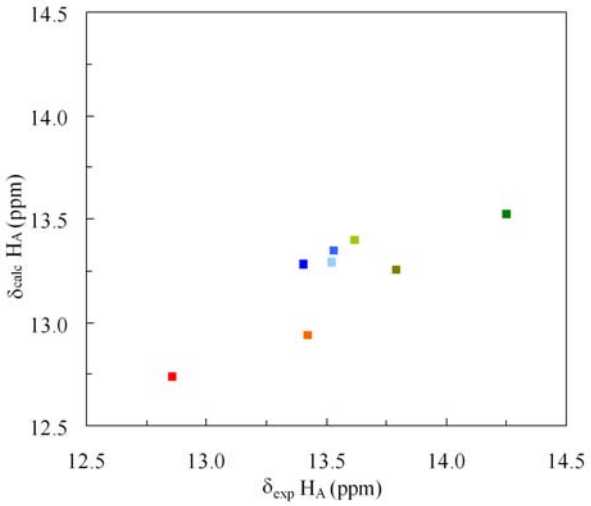


**Fig. 3** Plot of calculated $^1$H-NMR chemical shifts vs. experimentally observed $^1$H-NMR chemical shifts of the $H_A$ proton

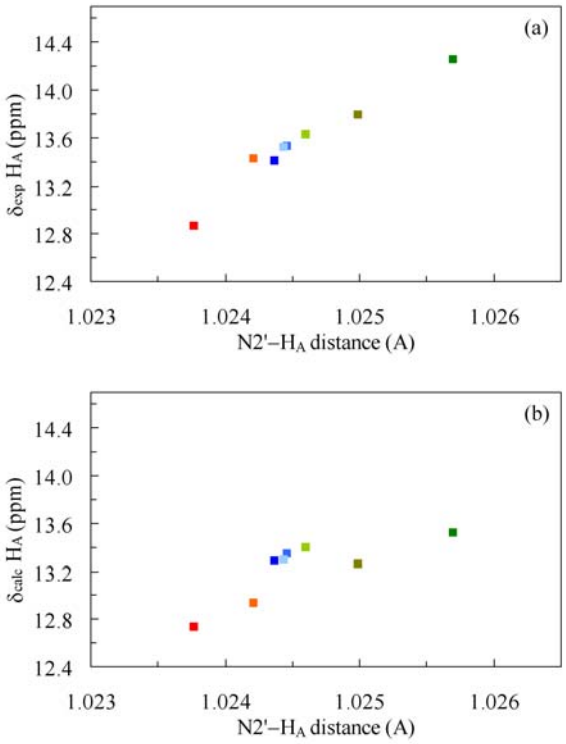


**Fig. 4** Plots of experimental (a) and calculated (b) $^1$H NMR chemical shift of $H_A$ vs. the N2′–$H_A$ internuclear distance.

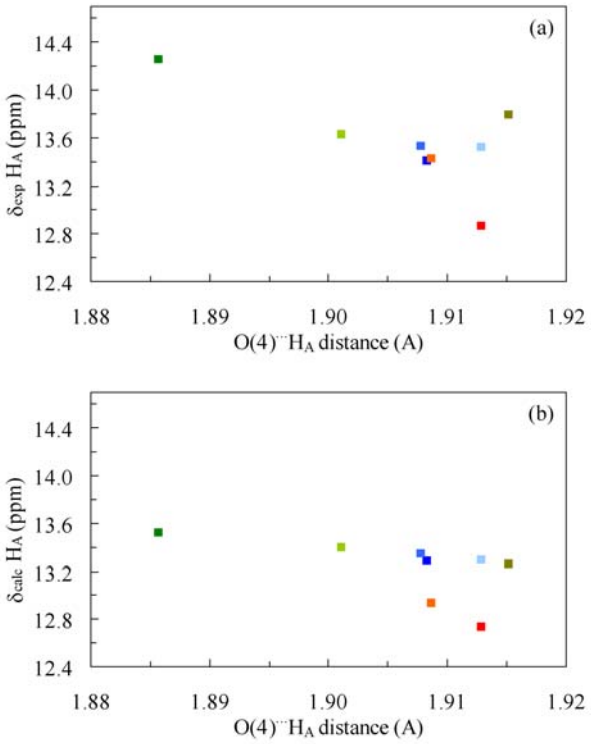


**Fig. 5** Plots of experimental (a) and calculated (b) $^1$H-NMR chemical shift of $H_A$ vs. the O(4)···$H_A$ internuclear distance.

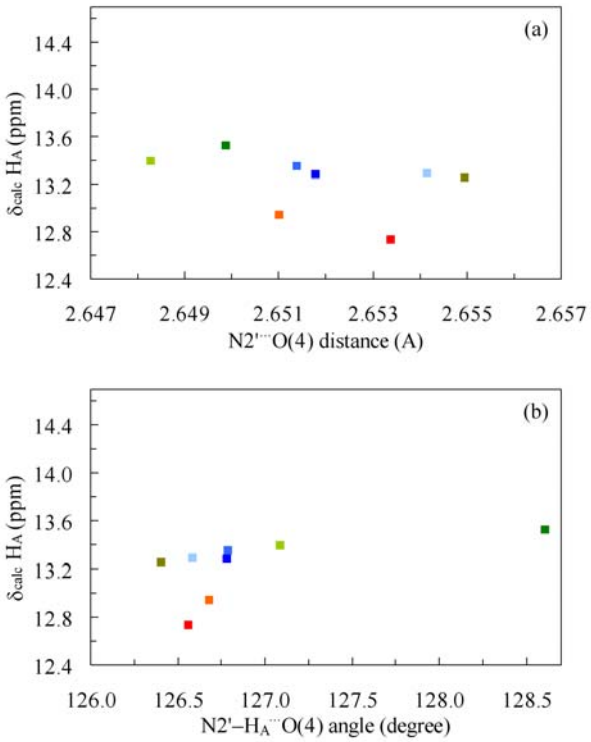


**Fig. 6** Plots of calculated $^1$H-NMR chemical shifts of $H_A$ vs. the N2′···O(4) internuclear distance (a) and the N2′–$H_A$···O(4) angle (b).

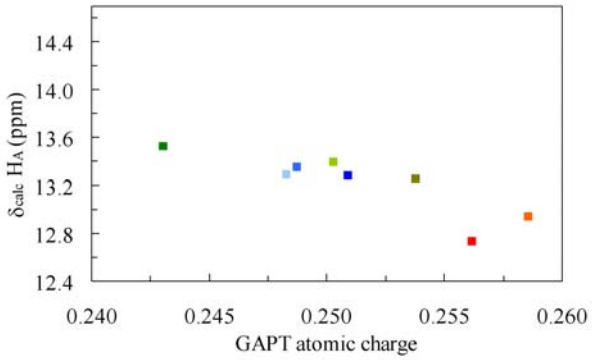


**Fig. 7** Plot of calculated $^1$H-NMR chemical shifts of $H_A$ vs. the calculated GAPT atomic charges of the $H_A$ proton.

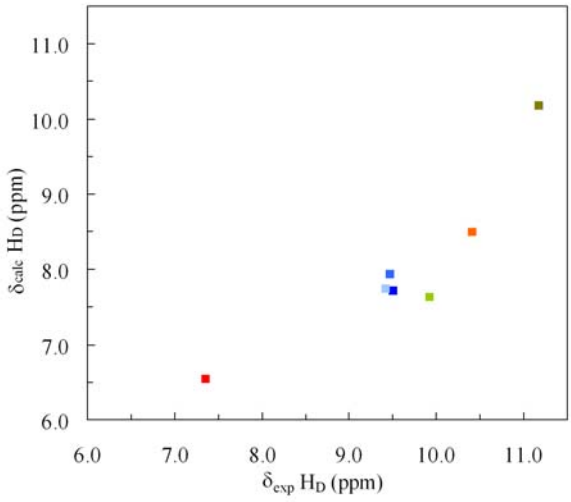


**Fig. 8** Plot of calculated $^1$H-NMR chemical shifts vs. experimentally observed $^1$H-NMR chemical shifts of the $H_D$ proton.

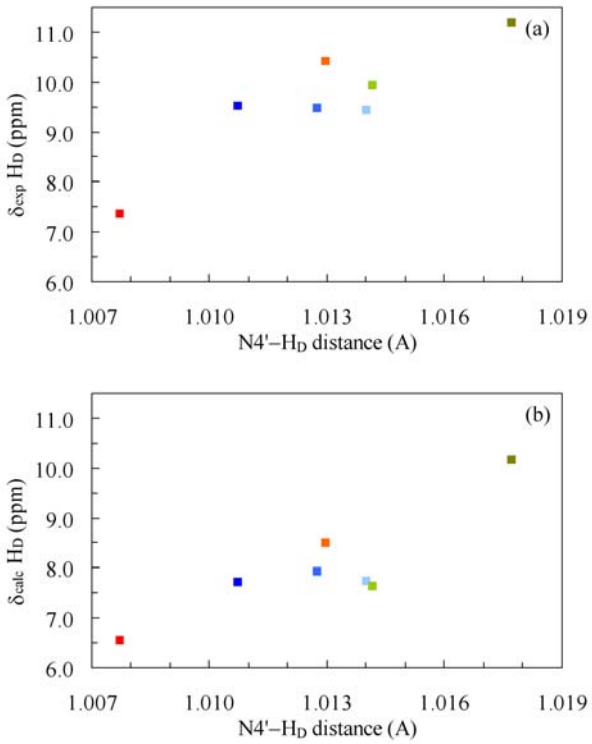


**Fig. 9** Plots of experimental (a) and calculated (b) $^1$H-NMR chemical shift of $H_D$ vs. the N4′–$H_D$ internuclear distance.

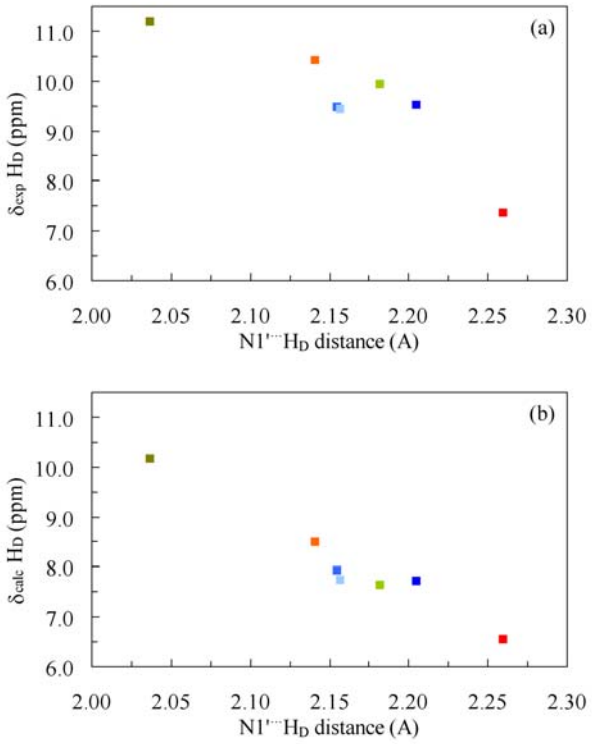


**Fig. 10** Plots of experimental (a) and calculated (b) $^1$H-NMR chemical shift of $H_D$ vs. the N1′···$H_D$ internuclear distance.

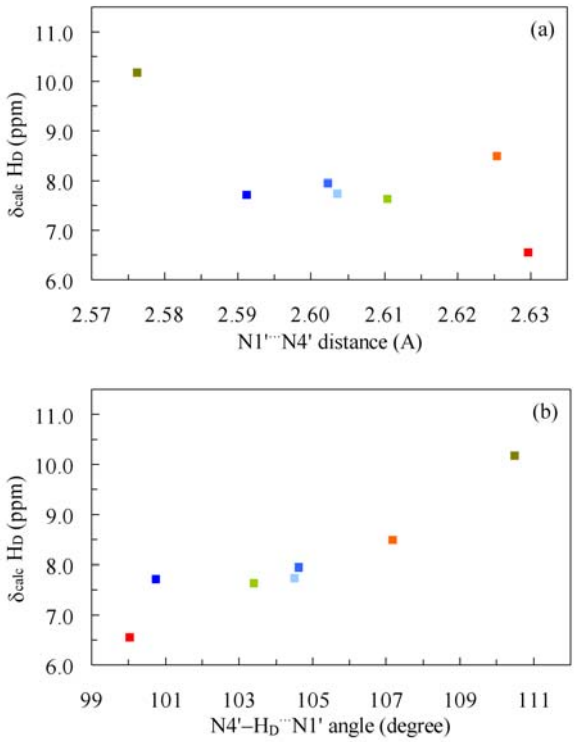


**Fig. 11** Plots of calculated $^1$H-NMR chemical shifts of $H_D$ vs. the N1′···N4′ internuclear distance (a) and the N4′–H$_D$···N1′ angle (b).

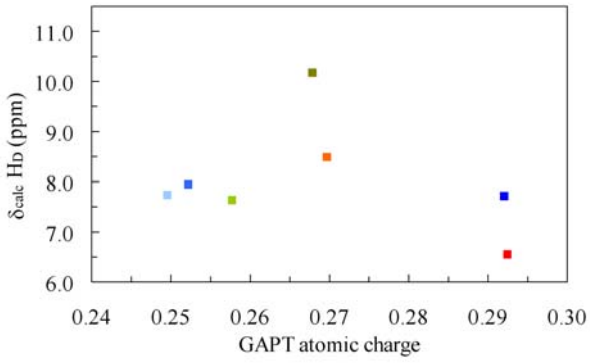


**Fig. 12** Plot of calculated $^1$H-NMR chemical shifts of $H_D$ vs. the calculated GAPT atomic charges of the $H_D$ proton.